Available online at www.sciencedirect.com
SCIENCE DIRECT®
Journal of Nuclear Materials 325 (2004) 107–117
journal of nuclear materials
www.elsevier.com/locate/jnucmat

A model for fission-gas-bubble behavior in amorphous uranium silicide compounds

J. Rest

Argonne National Laboratory, Energy Technology-212, 9700 S. Cass Avenue, Argonne, IL 60439-4815, USA

Received 11 August 2003; accepted 14 November 2003

Abstract

A model for the behavior of fission gas in irradiated amorphous materials is developed. The model proposes that gas bubble nucleation occurs within shear bands initiated around free volume regions. Small gas–atom clusters that form within these regions are susceptible to dissolution by forces generated by the plastic flow of material around the cluster. The bubble coarsening process depends on the materials viscosity and on irradiation-induced re-solution. The bubble distribution eventually reaches a point where larger bubbles from the tail of the evolving lognormal size distribution begin to contact the more numerous nanometer-sized bubbles from the peak region. This condition defines the knee in the swelling curve. The fission density at which the knee occurs is a function of fission rate. Calculations for the behavior of the knee, swelling, and the fraction of gas in bubbles in irradiated U_3Si_2 intermetallic compounds are compared to measured quantities.

1. Introduction

Low-enriched uranium–silicide dispersion fuel is used extensively worldwide in research and test reactors. Previous post-irradiation examinations of the material had indicated that the material remained crystalline to high fission doses. A model for irradiation-induced recrystallization of U_3Si_2 (and UO_2) was developed and successfully applied to the interpretation of the experimental observations [1]. Subsequently, ion irradiation and neutron diffraction studies [2] did not confirm the crystalline interpretation, but instead demonstrated that the as-fabricated crystalline material transformed rapidly upon irradiation to an amorphous state and remained thus to extremely high fission doses [3].

In stable intermetallic compounds such as U_3Si_2 (e.g., as compared to compounds such as U_3Si that exhibit unstable swelling behavior), the fission gas bubble morphology is uniform with no clear evidence of bubble coalescence or inter-linkage. The small fission gas bubbles remain stable to high burn-up. Even at 63% burn-up of a 93% enriched mini-plate, the fission gas bubbles retain a uniform morphology [1].

Two very important observations were made that still underpin current understanding of the swelling behavior [1]. Firstly, the initial rate of swelling is relatively low, and then accelerates markedly. This transition referred to as the 'knee point' marks the fission density at which the fission gas bubbles reach a sufficient size to influence swelling behavior in addition to solid fission products. Prior to the knee, a small fraction of the fission gas is retained in solution while the rest is believed to be stored in nanometer-size bubbles which are below the limit of resolution of the SEM. Secondly, the fission rate appeared to influence the fission density at which the fuel swelling began to accelerate. At a higher fission rate the knee point is shifted to a higher fission density.

The paper is organized as follows. Section 2 contains the model description. The model consists of a set of rate equations that are described in Section 2.1 and solved

E-mail address: jrest@anl.gov (J. Rest).

0022-3115/$ - see front matter © 2003 Elsevier B.V. All rights reserved.
doi:10.1016/j.jnucmat.2003.11.008

numerically in Section 3 in order to extract time dependencies. Next analytical approximations are obtained in Section 2.2 in order to facilitate interpretation of predicted behavior. Section 2.3 contains an evaluation of the steady-state bubble-size distribution in order to evaluate critical quantities required in the rate-theory and analytical solution formulations. Finally, Sections 2.4 and 2.5 contain an analysis of bubble growth at and beyond the knee. Section 3 consists of a comparison of the theory with data for an U_3Si_2 intermetallic compound. Discussion and conclusions are presented in Section 4.

2. Model description

2.1. Constitutive equations

In crystals bubbles cannot form without vacancies. Vacancy migration leads to bubble growth. This basic mechanism still holds for amorphous materials. In amorphous materials fission damage does not produce vacancies but instead generates free space commonly called free volume. Fission gas generated during irradiation diffuses by a free volume migration mechanism and leads to the nucleation and growth of fission gas bubbles. The diffusivity of the gas in the amorphous material can be described by a Nernst–Einstein relationship [4], i.e. the diffusivity is inversely proportional to the viscosity η,

$$D_g = \frac{kT}{6\pi r_g \eta}, \tag{1}$$

where T is the absolute temperature, k is Boltzmann's constant, and r_g is the radius of a diffusing gas–atom. A drastic decrease in the viscosity of a simple glass has been observed to occur under irradiation by heavy ions [5,6]. In analogy with mechanical deformation, the viscosity is assumed to have a similar dependence on fission rate as it has on mechanically induced strain rate, i.e. the viscosity is inversely proportional to the fission rate $\dot{f}$,

$$\eta = \eta_0/\dot{f}, \tag{2}$$

where in general η_0 is a function of temperature, i.e. $\eta_0 = e^{-\theta/T}$. Eq. (2) is supported by observations of plastic flow of glasses under bombardment by heavy ions [6]. Combining Eqs. (1) and (2) results in a gas–atom diffusivity that is proportional to the fission rate, i.e.

$$D_g = \frac{kT\dot{f}}{6\pi r_g \eta_0} = D_0 \dot{f}, \tag{3}$$

where $D_0 = D_0(T) = kT/6\pi r_g \eta_0$. Free volume migration can also result in the movement of small bubbles by a volume diffusion mechanism. In this case the gas-bubble diffusivity is given by

$$D_b = \frac{3\Omega D_g}{4\pi r_b^3}, \tag{4}$$

where Ω is the atomic volume and r_b is the bubble radius.

The bubble nucleation rate is proportional to the interaction rate between fission gas atoms. In general, when gas atoms come together at a free volume site in the amorphous material and form a small cluster, neighboring host atoms produce interactions with the cluster that can lead to its dissolution. For example, consider the mechanism of plastic flow in metallic glasses in which strain is produced by the local rearrangement of atoms nucleated under the applied stress with the assistance of thermal fluctuations in regions around free volume sites. Argon named this strain generating mechanism a local shear transformation [7]. During these local shear transformations the surrounding atoms have to be pushed apart at some point along the activation path, producing an activation dilatation. If the small gas atom clusters are nearby to the dilatation, nucleation of a gas bubble can occur. Thus, the bubble nucleation rate depends on the volume fraction of shear bands in the material. This condition is analogous to the requirement in crystalline material that in order to become a stable bubble, the gas atom clusters must be in close proximity to vacancies and/or vacancy clusters [8]. Bubble nucleation is not considered to occur outside of the shear bands due to insufficient free volume within the U_3Si_2 compound (e.g., U_3Si_2 contracts upon amorphization: see Ref. [2]).

Consider a region of the material initially shearing at a rate $\dot{\gamma}_0$ imposed by some external agency that maintains the rate constant. The separation of flow in this region into shear bands covering a fraction f_s of the volume and the remaining matrix covering a fraction $(1 - f_s)$ is described by the equation

$$f_s\dot{\gamma}_b + (1 - f_s)\dot{\gamma}_m = \dot{\gamma}_0. \tag{5}$$

In general, $\dot{\gamma}_m \ll \dot{\gamma}_0 \ll \dot{\gamma}_b$ so that solving Eq. (5) for f_s yields

$$f_s \approx \frac{1}{\dot{\gamma}_b}\left(\dot{\gamma}_0 - \dot{\gamma}_m\right) \approx \frac{\dot{\gamma}_0}{\dot{\gamma}_b} = \frac{\alpha}{\dot{f}}. \tag{6}$$

The shear strain rate $\dot{\gamma}_b$ in Eq. (6) due to mechanical deformation has been assumed to be proportional to the fission rate $\dot{f}$, where α is the constant of proportionality. This last relationship underlies the assumption that there is a direct correspondence between mechanically induced and fission-induced processes in the same material (i.e., in one the stresses are induced by mechanical deformation and in the other by fission events).

Eq. (2) gives the viscosity of an amorphous material undergoing shear deformation due to fission spikes. We are concerned here with the behavior of bubble nucleation as a function of fission rate, or analogously, viscosity. As the fission rate increases, the viscosity decreases and, thus, the shear strain rate within the shear bands increases. Eq. (6) states that for constant $\dot{\gamma}_0$, an increase in $\dot{\gamma}_b$ results in a smaller volume fraction of shear bands in the material.

When gas atoms come together within a free volume site, a shear force acting to separate the atoms is generated by the plastic flow of material around the cluster. These small gas–atom clusters must grow to a critical size (e.g., on the order of 10 or more gas atoms) in order to become a stable, equilibrium gas bubble. In analogy with the theory of viscous adhesion [9], it is assumed that the probability that the gas–atom cluster stays intact is proportional to the viscosity. Thus, the bubble nucleation rate is proportional to the viscosity as well as to f_s, i.e.

$$\frac{dc_b(t)}{dt} \approx f_s \eta, \tag{7}$$

where c_b is the gas-bubble concentration.

As the irradiation continues, the bubble-size distribution coarsens by bubble growth due to the accumulation of fission gas atoms and bubble coalescence. In addition, bubbles can be totally destroyed (whole bubble destruction for bubbles below a critical size) by collisions with fission fragments, or have their growth rate reduced due to the shrinkage effects of irradiation-induced re-solution. With the exception of the bubble nucleation mechanism given by Eqs. (2) and (7), the equations describing the time evolution of the fission gas atoms and bubbles in the amorphous compound are analogous to the rate equations describing bubble behavior in a crystalline material [10] and are given by

$$\frac{dc_g(t)}{dt} = \beta \dot{f} - \frac{4\pi f_n D_g c_g(t) c_g(t)}{\dot{f}^2} - 4\pi r_b(t) D_g c_b(t) c_g(t) + 2b m_b(t) c_b(t), \tag{8}$$

$$\frac{dc_b(t)}{dt} = \frac{4\pi f_n D_g c_g(t) c_g(t)}{m_b(t)\dot{f}^2} - b c_b(t) - 16\pi r_b(t) D_b(t) c_b(t) c_b(t), \tag{9}$$

$$\frac{dm_b}{dt} = 4\pi r_b(t) D_g c_g(t) - b m_b(t) + 16\pi r_b(t) D_b(t) m_b(t) c_b(t), \tag{10}$$

where c_g and c_b are the concentration of gas atoms and bubbles, respectively, m_b is the number of gas atoms in a bubble of radius r_b, b is the gas–atom re-solution rate, and $f_n = 4\alpha\eta_0 r_g$.

The quantities c_g, c_b, m_b in Eqs. (8)–(10) represent average values. For example, $c_b(t)$ bubbles each containing $m_b(t)$ gas atoms represents the average value of the bubble-size distribution at time t. In general, r_b is related to m_b through the gas law and the capillarity relation. Using the van der Waals gas law,

$$\frac{2\gamma}{r_b}\left(\frac{4}{3}\pi r_b^3 - b_v m_b\right) = m_b k T, \tag{11}$$

where γ is the surface tension, b_v is the van der Waals constant, k is Boltzmann's constant, and T is the absolute temperature. The four terms on the right-hand-side of Eq. (8) respectively represent the generation of gas atoms due to fission (β is the number of gas atoms produced per fission), the loss of gas atoms due to bubble nucleation, the loss of gas atoms due to diffusion to existing bubbles, and the gain of gas atoms due to irradiation-induced gas–atom re-solution from bubbles. The three terms on the right-hand-side of Eq. (9) respectively represent the gain of bubbles due to bubble nucleation, the loss of bubbles due to whole bubble destruction by interaction with fission fragments, and the loss of bubbles due to bubble coalescence. The three terms on the right-hand-side of Eq. (10) respectively represent the gain of gas atoms per bubble due to gas atom diffusion to bubbles, the loss of gas atoms per bubble due to irradiation-induced re-solution, and the gain of gas atoms per bubble due to bubble coalescence. In general, the gas–atom re-solution rate is proportional to the fission rate, i.e.

$$b = b_0 \dot{f}. \tag{12}$$

Eqs. (8)–(11) can be solved numerically to obtain the quantities $c_g(t)$, $c_b(t)$, $m_b(t)$, and $r_b(t)$. Results obtained from their solution will be shown in Section 3. However, it is instructive to qualitatively describe these results in order to obtain approximate analytical solutions to these equations.

Due to the strong effect of irradiation-induced gas–atom re-solution, in the absence of geometrical contact the bubbles stay in the nanometer size range. The density of bubbles increases rapidly early in the irradiation. Subsequently, at longer times the increase in bubble concentration occurs at a much-reduced rate at the relatively low irradiation temperatures under consideration ($T/T_m < 0.5$).

Eventually, the bubble distribution reaches a point where larger bubbles from the tail of the distribution begin to contact the more numerous smaller bubbles from the peak region. This condition defines the knee in the swelling curve. That these nanometer-sized bubbles exist and have an evolving size-distribution that is consistent with the above picture is clearly illustrated in Fig. 1 that shows a TEM photograph of bubble formation

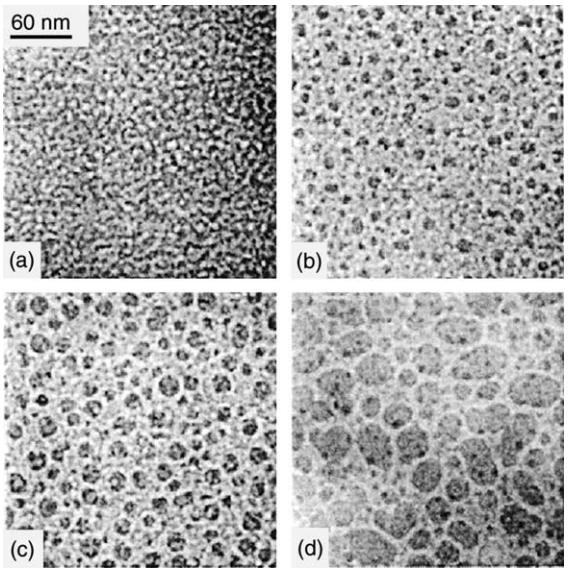

Fig. 1. Images taken from an area of a Na–borosilicate glass sample that was implanted by 50 keV Xe at 200 °C with different doses: (a) 1.0×10^{20} ion/m^2; (b) 1.2×10^{20} ion/m^2; (c) 1.3×10^{20} ion/m^2; (d) 1.4×10^{20} ion/m^2 [11].

and growth in glasses [11]. The validity of an evolving log normal bubble-size distribution in an irradiated amorphous material that coarsens by bubbles growing into each other is further strengthened by the observation of nanometer sized helium bubbles that form, grow, and coalesce during low-temperature helium implantation in an amorphous alloy [12].

2.2. Analytical approximations

Approximate analytical solutions to Eqs. (8)–(11) are derived in this section in order to facilitate interpretation of predicted behavior. Based on the argument given above regarding the much reduced rate of the bubble density at longer irradiation times, the left-hand-side of Eq. (9) is set equal to zero and the last term on the right-hand-side is dropped. Again, this approximation will be more reasonable for larger values of t. A solution for c_b in terms of m_b and t is given by

$$c_b = \frac{4\pi f_n D_0 \dot{f} \beta_e^2 t^2}{b_0 m_b(t)}, \tag{13}$$

where Eqs. (3) and (12), and an approximate solution to Eq. (8) have been used, i.e.

$$c_g = \beta_e \dot{f}^{3/2} t. \tag{14}$$

The validity of Eq. (14) is examined in Section 3. For bubbles in the nanometer size range an approximate solution to Eq. (11) is given by setting the quantity in brackets equal to zero, i.e.

$$r_b(t) = \left(\frac{3 b_v m_b(t)}{4\pi}\right)^{1/3}. \tag{15}$$

Using Eq. (15) and neglecting the last term in Eq. (10) an equation for dr_b/dt can be written as

$$\frac{dr_b(t)}{dt} = \frac{b_v D_0 \dot{f}^{5/2} \beta_e t}{r_b(t)} - \frac{b r_b(t)}{3}. \tag{16}$$

Eq. (16) can be integrated to obtain

$$r_b = \left(\frac{3\beta_e b_v D_0 \dot{f}^{3/2} t}{b_0}\right)^{1/2}, \tag{17}$$

where Eq. (12) has been utilized. The solution for c_b can now be expressed as

$$c_b = \frac{f_n}{\dot{f}^{5/4}} \sqrt{\frac{b_0 \beta_e t}{3 b_v D_0}}. \tag{18}$$

From Eq. (18), the rate of change of c_b with respect to t is proportional to $t^{-1/2}$. Thus, dc_b/dt decreases as t increases. The approximation used in obtaining Eq. (18) is thus reasonable at relatively high values of t.

Bubble nucleation occurs primarily at relatively early times in the irradiation. Subsequently, coarsening of the distribution occurs by bubble growth due to accumulation of fission gas atoms that diffuse to the bubbles. At some point larger bubbles from the tail of the bubble-size distribution growing will contact smaller bubbles and a mass coalescence event will be initiated. This point is defined as the 'knee'. This nomenclature comes about due to the fact that once the mass coalescence event has taken place the swelling curve will show an increase in slope as a function of dose. For a homogeneous, isotropic distribution of spherical bubbles, contact is achieved when the ratio of the bubble diameter to inter-bubble spacing is equal to one. For bubble distributions that are not homogeneous and/or for bubbles that are not spherical, contact is achieved for values of this ratio less than one. The ratio of bubble diameter to inter-bubble spacing is given by

$$R_{ds} = 2 r_b c_b^{1/3}. \tag{19}$$

Using Eqs. (17) and (18), Eq. (19) becomes

$$R_{ds} = 2\left[\frac{3 f_n D_0 \beta_e^2 \dot{f} b_v t^2}{b_0}\right]^{1/3}. \tag{20}$$

Defining the value of this ratio at which the knee is reached as R_{ds}^{crit}, the fission density at which the threshold achieved is obtained by solving for $\dot{f}t$ in Eq. (20) and is given by

$$(\dot{f}t)_{\text{knee}} = \left[\frac{b_0}{24 f_n D_0 b_v}\right]^{1/2} \frac{\sqrt{\dot{f}}}{\beta_e} (R_{ds}^{\text{crit}})^{3/2}, \tag{21}$$

where R_{ds}^{crit} is a property of the bubble-size distribution.

The fraction of fission gas generated that exists in bubbles is given approximately by

$$\chi(t) = \frac{m_b(t) c_b(t)}{\beta \dot{f} t}. \tag{22}$$

Using Eqs. (15), (17), and (18), Eq. (22) becomes

$$\chi(t) = \frac{4\pi f_n D_0 \beta_e^2 t}{b_0 \beta}. \tag{23}$$

The value of χ at $(\dot{f}t)_{\text{knee}}$ is given by

$$\chi_{\text{knee}} = \frac{4\pi f_n \beta_e^2 D_0 (\dot{f}t)_{\text{knee}}}{b_0 \beta \dot{f}}. \tag{24}$$

In terms of R_{ds}^{crit}, Eq. (24) becomes

$$\chi_{\text{knee}} = \frac{2\pi \beta_e \left(R_{ds}^{\text{crit}}\right)^{3/2}}{\beta} \sqrt{\frac{f_n D_0}{6 \dot{f} b_v b_0}}. \tag{25}$$

2.3. Determination of R_{ds}^{crit}

2.3.1. Calculation of the bubble-size distribution

The knee in the swelling curve has been ascribed in the model described above to the regime wherein the interconnection of the nanometer size bubble population occurs. As the dynamics of bubble interconnection depend, in general, on the characteristics of the bubble-size distribution it is first necessary to obtain an expression for this quantity.

Let $n(r)\,dr$ be the number of bubbles per unit volume with radii in the range r to $r + dr$. Growth by gas atom collection removes bubbles from this size range, but these are replaced by the simultaneous growth of smaller bubbles. A differential growth rate between bubbles of different size leads to a net rate of increase in the concentration of bubbles in the size range r to $r + dr$. This behavior is expressed by [13]

$$\left[\frac{dn(r)}{dt}\right] dr = \frac{d}{dr}\left[n(r)\frac{dr}{dt}\right] dr. \tag{26}$$

The growth rate (dr/dt) of a particular bubble is related to the rate (dm/dt) at which it absorbs gas from the matrix. The rate of precipitation is controlled by the gas–atom diffusion coefficient D_g and the average concentration c_g of fission gas retained in the lattice,

$$(dm/dt) = 4\pi D_g r c_g. \tag{27}$$

For small bubbles, the relationship between size and gas content can be approximated by

$$m(r) = (4\pi r^3/3 b_v). \tag{28}$$

Differentiating Eq. (28) and equating to Eq. (27) results in

$$dr/dt = b_v D_g c_g / r. \tag{29}$$

The rate of bubble shrinkage due to irradiation-induced re-solution is given by

$$\left[\frac{dn(r)}{dt}\right] dr = -b_0 \dot{f} n(r)\, dr. \tag{30}$$

The overall net rate of change of the concentration of bubbles in a given size range is derived by subtracting the right-hand-side of Eq. (30) from that of Eq. (26):

$$\frac{dn(r)}{dt}\, dr = \frac{d}{dr}\left[n(r)\frac{dr}{dt}\right] dr + b_0 \dot{f} n(r)\, dr. \tag{31}$$

The equilibrium population of bubbles is obtained by setting Eq. (31) to zero

$$(b_v D_g c_g / r^2) n(r) - (b_v D_g c_g / r)\, dn(r)/dr - b_0 \dot{f} n(r) = 0, \tag{32}$$

where Eq. (29) has been used for dr/dt.

Eq. (32) must be solved subject to the relevant boundary condition. Here, because detailed information on bubble nucleation is not available, a constraint is imposed that the total number of gas atoms in the bubbles, i.e. the integral of $m(r)n(r)\,dr$ from r_0 to infinity is equal to a given fraction χ of the total gas generated during the time required to reach the knee, i.e. $t = t_{\text{knee}}$ and

$$\int_{r_0}^{\infty} m(r) n(r)\, dr = \chi \beta \dot{f} t, \tag{33}$$

where β is the number of gas atoms per fission. The solution to Eq. (32) with the boundary condition given by Eq. (33) is thus obtained as

$$n(r) = \frac{2 b_v \chi \beta \dot{f} t}{\pi^{3/2}} \kappa^{5/2} r \exp[-\kappa r^2], \tag{34}$$

where $\kappa = \kappa(t) = b_0/2\beta b_v D_g t$ and r_0 has been taken equal to zero. The total number of bubbles at the knee is given by

$$N_{\text{tot}} = \int_0^{\infty} n(r)\, dr = \frac{b_v \chi \beta \left(\dot{f} t\right)_{\text{knee}}}{\pi^{3/2}} \kappa^{3/2}. \tag{35}$$

The average size of a bubble within this distribution is given by

$$\bar{r} = \frac{1}{N_{\text{tot}}} \int_0^{\infty} r n(r)\, dr = \frac{1}{2}\sqrt{\frac{\pi}{\kappa}}. \tag{36}$$

Finally, the ratio of the average diameter of a bubble to the average inter-bubble spacing is

$$R_{ds} = 2\bar{r} N_{\text{tot}}^{1/3} = \left(b_v \chi \beta \dot{f} t\right)^{1/3} = \left(\frac{\chi b_0}{2 D_0 \kappa}\right)^{1/3}. \tag{37}$$

2.3.2. Calculation of bubble–bubble contact

As the bubble-size distribution coarsens larger bubbles of the distribution intersecting smaller bubbles will initiate interconnection. This event will lead to a volume increase due to bubble–bubble coalescence and act as an initiator of subsequent coalescence events. The overall process will result in bubble clustering with the eventual formation of a single large bubble within the localized fuel volume. In general, interconnection can be described as the condition where the average number of intersections a given bubble makes with other bubbles is greater or equal to 2. However, for the situation described above, due to the volume increase associated with bubble coalescence the average number of intersections required for the initiation of bubble interconnection can be less then 2.

A spherical bubble of radius R suspended in a system containing the bubble-size distribution given by Eq. (34) will be touched by those spheres of radius r whose centers are less than $(r+R)$ away from the center of the sphere under consideration. The mean number of other spheres $\bar{I}$ by which the given sphere of radius R is intersected is therefore equal to the sum over r of the probability of finding centers of spheres within a volume of radius $(r+R)$, i.e.

$$\begin{aligned}\bar{I}(R) &= \frac{4\pi}{3}\int_0^\infty (r+R)^3 n(r)\,\mathrm{d}r \\ &= \frac{b_v \chi\beta\dot{f}t}{3\pi^{1/2}}\left(4r\sqrt{\kappa}(3+\kappa R^2)+\sqrt{\pi}(3+6\kappa R^2)\right) \\ &= \frac{\chi b_0}{6\pi^{1/2}D_0\kappa}\left(4r\sqrt{\kappa}(3+\kappa R^2)+\sqrt{\pi}(3+6\kappa R^2)\right).\end{aligned} \tag{38}$$

The purpose of the above formulation is to develop a relationship between the parameter R_{ds} that is used to set the position of the knee given by Eq. (21) within the rate-theory formulation expressed in Eqs. (8)–(10) and properties of the bubble-size distribution that determine the onset of interconnection, i.e. as expressed by Eq. (38). To this end let $I(r_I)$ be the mean number of other spheres by which a given sphere of radius r_I must intersect in order to initiate interconnection of the bubble-size distribution. By definition, this is the knee in the swelling curve ($t = t_{knee}$). Solving Eq. (37) for κ and substituting into Eq. (38)

$$\begin{aligned}\bar{I}(r_I) = \frac{R_{ds}^3}{6\pi^{1/2}}\Bigg(&4\sqrt{\frac{\chi b_0}{D_0}\frac{r_I^2}{R_{ds}^3}}\left(3+\frac{\chi b_0}{D_0 R_{ds}^3}r_I^2\right) \\ &+\sqrt{\pi}\left(3+6\frac{\chi b_0}{D_0 R_{ds}^3}r_I^2\right)\Bigg).\end{aligned} \tag{39}$$

If $y = \bar{I}(r_I)/r_I^2$ and $x = r_I^2/R_{ds}^3$ then Eq. (39) can be rewritten as

Table 1
Values of parameters used in calculation for U_3Si_2

Parameter	Value	Reference
β	0.25	[8]
β_e	5.6×10^{-12} m$^{3/2}$ s$^{1/2}$	This work
b_0	2×10^{-23} m^3	[14]
η_0	$2\times10^{7}\ \dot{f}_0$ poise	This work
r_g	0.216 nm	[1]
γ	0.7 J m^{-2}	[15]
$\dot{f}_0$	1.25×10^{20} m^{-3} s^{-1}	This work
α	$5\times10^{-10}\ \dot{f}_0$	This work
β_s	1.75×10^{-29} m^3	This work
ϕ	8×10^{-8} s^{-1}	This work

$$y = \frac{1}{6\pi^{1/2}x}\left(4\sqrt{\frac{\chi b_0}{D_0}x}\left(3+\frac{\chi b_0}{D_0}x\right)+\sqrt{\pi}\left(3+6\frac{\chi b_0}{D_0}x\right)\right). \tag{40}$$

The expected value of $\bar{I}(r_I)$ is of order unity. For a given r_I the intersection of graphs of the left and right side of Eq. (40) yields the value of R_{ds}. Table 1 shows values of the parameters used to perform the calculation for U_3Si_2 intermetallic compound. As discussed in the next section, the tail of the lognormal bubble-size distribution given by Eq. (34) is defined to initiate at a bubble radius $r_I = 3.33r_{peak}$. r_I is the smallest bubble within the tail region, and thus, all bubbles within the tail will participate in contact coalescence for $\bar{I}(r_I) = 1$. For this value of r_I the solution of Eq. (40) yields a value of $R_{ds} = 0.42$.

2.4. Bubble growth at the knee

At the knee the larger bubbles within the tail of the bubble-size distribution begin to contact smaller bubbles and grow as a result of the coalescence. This growth facilitates more contact and the process continues until the density of smaller bubbles is reduced below the value required for contact. In order to simplify a quantitative description of this process, the bubble-size distribution is separated into two regimes characterized by average radii and number densities: the small bubble bell-shaped region, and the large bubble tail region. The peak of the bubble-size distribution given by Eq. (34) occurs at a bubble radius

$$r_{peak} = \sqrt{\frac{1}{2\kappa}}. \tag{41}$$

The bubble radius that defines the interface between the two regions r_I (see Fig. 3) is taken to be

$$r_I = 3.33r_{peak}. \tag{42}$$

The tail of the bubble-size distribution is centered at a bubble radius

$$r_{\text{tail}} = 5r_{\text{peak}}. \tag{43}$$

The average bubble densities characterizing these two regions are obtained by integrating Eq. (34) over each regime to obtain, respectively, the total quantity of gas in bubbles and choosing number densities of bubbles of sizes r_{peak} and r_{tail}, respectively that are consistent with the conservation of gas atoms, i.e.

$$N_1 = \frac{1}{m(r_{\text{peak}})}\int_0^{r_1} m(r)n(r)\,\mathrm{d}r = 3.6\chi b_{\text{v}}\beta\dot{f}t\left(\frac{\kappa}{\pi}\right)^{3/2}, \tag{44}$$

$$N_2 = \frac{1}{m(r_{\text{tail}})}\int_{r_1}^{\infty} m(r)n(r)\,\mathrm{d}r = 2\times 10^{-3}\chi b_{\text{v}}\beta\dot{f}t\left(\frac{\kappa}{\pi}\right)^{3/2}, \tag{45}$$

where the ideal gas law (i.e., neglect second term within the parenthesis in Eq. (11)) has been used to express $m(r)$ and $m(r_{\text{tail}})$ in Eq. (45) in order to simplify the integration.

Fig. 2 shows $n(r)$ from Eq. (34) as well as the position of r_{peak}, r_{I}, and r_{tail} calculated at the onset of the knee for a fission rate of 2.5×10^{20} $\text{m}^{-3}\,\text{s}^{-1}$ and using the parameters in Table 1. The insert in Fig. 2 is a blowup of the region containing r_{I} and r_{tail} showing details of their positioning. Fig. 3 shows the calculated (Eq. (39)) average number of intersections of a bubble with radius r_{I} with other bubbles in distribution $n(r)$ shown in Fig. 2. The position of $\bar{I}(r_{\text{I}}) = 1$ is shown and corresponds to the onset of the knee and to the value of $R_{\text{ds}} = 0.42$ obtained from the solution of Eq. (40).

The coarsening of the larger bubbles in region 2 at the expense of the smaller bubbles in region 1 is modeled by an increase in the radius R of a fixed density of N_2 bubbles with a commensurate decrease in the density N

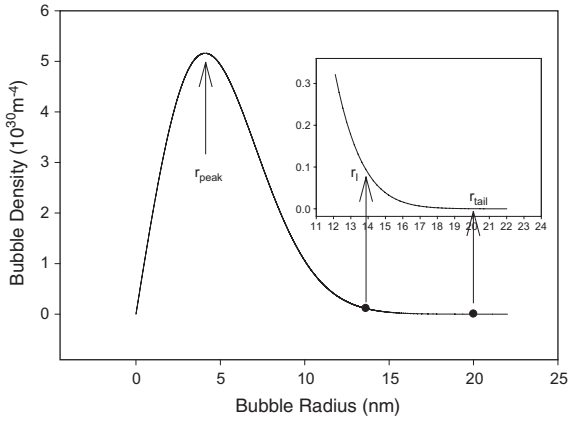

Fig. 2. Calculation of bubble-size distribution showing position of r_{peak}, r_{I} and r_{tail}. The inset shows a blowup of the region containing r_{I} and r_{tail}.

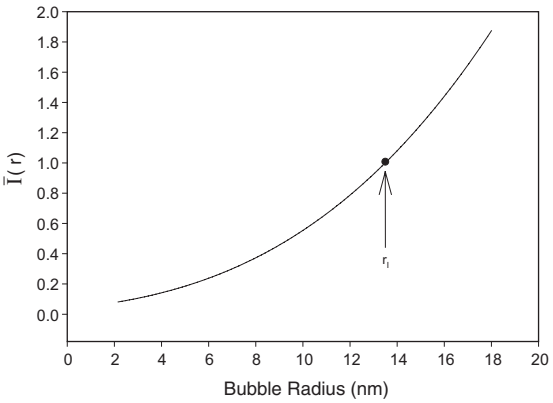

Fig. 3. Calculation of average number of intersections of bubble with radius r_{I} with other bubbles in distribution $n(r)$ shown in Fig. 2. The position of $\bar{I}(r_{\text{I}}) = 1$ is shown and corresponds to the onset of the knee and to the value of $R_{\text{ds}} = 0.42$ obtained from the solution of Eq. (40).

of bubbles having fixed radius r_{peak}. If the population of N_1 bubbles decreases by ΔN_1 due to coalescence with the population of N_2 bubbles, the number of gas atoms in N_2 bubbles increases from $m(r_{\text{peak}})$ to $m(\text{obs})$ where

$$m(\text{obs}) = m(r_{\text{tail}}) + m(r_{\text{peak}})\Delta N_1/N_2. \tag{46}$$

The bubble density functions $n(r)$, (r_{peak}, N_1), and (r_{tail}, N_2) represent spatially smeared quantities: the bubble density is locally high in some regions and locally low in others. Coalescence at the knee will continue until all of the locally high bubble density regions are consumed with each local region being replaced by one bubble containing $m(\text{obs})$ gas atoms. At this point the bubble-size distribution (e.g., Eq. (34)) will represent the remaining spatial regions. It is assumed here that the characteristics of the bubble-size distribution are such that when the locally high-density regions are removed from the calculation, the average number of intersections a representative bubble at the interface between the two regions has with other bubbles (Eq. (38)) is equal to 1/2. This condition constrains the larger bubbles in the tail to have an average number of intersections with other bubbles <1, and the contact-coalescence event is terminated. It follows from Eq. (38) that, in terms of the average quantities in regions 1 and 2 this condition is satisfied by

$$\Delta N_1 = \frac{N_1}{2}. \tag{47}$$

2.5. Bubble growth after the knee

Eqs. (45)–(47) can be solved to obtain the radius of the large bubble distribution after the coalescence event at the knee reaches completion, i.e.

$$R = \frac{1}{2}\left[\frac{50}{\kappa} + \frac{196\pi kT}{\gamma b_v \kappa^{3/2}}\right]^{1/2}. \quad (48)$$

Immediately after knee formation the gas bubble swelling is given by

$$\left(\frac{\Delta V}{V_0}\right)_g^{t=t_{knee}} = \frac{4\pi}{3}\left(r_{peak}^3 \frac{N_1}{2} + R^3 N_2\right). \quad (49)$$

Subsequent to the formation of the knee the above process repeats, but now the evolution of the nanometer size bubble distribution is overlaid on the pre-existing larger bubble population. Both bubble distributions coarsen due to the accumulation of fission gas as the irradiation proceeds. Eventually, a secondary knee point is achieved and a second population of bubbles in the tenths of a micron size range is generated. Thus, as the population of larger bubbles formed at the primary knee has coarsened, a bi-modal population of bubbles is observed subsequent to the secondary knee point.

The spatial distribution of larger bubbles formed at the knee by coalescence of clusters of smaller bubbles growing into each other mirrors the spatial distribution of the bubble distribution prior to the knee, but on a larger length scale. Thus, as the irradiation proceeds, larger bubbles situated in relatively close proximity will grow into each other and coalesce. The rate of swelling increases at the knee due to the large bubble coarsening process. The large bubble coarsening process is described by

$$N(t) = N_2 e^{-\phi(t-t_{knee})}, \quad (50)$$

where the value of the rate constant ϕ is estimated from the data (see Table 1).

The interpretation provided for Fig. 5 (discussed in Section 3, below) that the fraction of generated gas in bubbles remains relatively constant after knee formation supports the assumption that the generated gas is depleted initially by the evolving nanometer size bubble distribution with the remainder available for absorption into the existing, larger bubble population. Thus, for times $t > t_{knee}$ the growth of the larger bubbles can be expressed by

$$\frac{dm(t)}{dt} = \frac{[1-\chi(t)]\beta\dot{f}}{N(t)} - \frac{m(t)}{N(t)}\frac{dN(t)}{dt}, \quad (51)$$

where $\chi(t) \leqslant \chi(t_{knee})$.

Eqs. (50) and (51) can be solved to obtain $m(t)$. Thus, the fuel swelling after knee formation is approximately given by

$$\left(\frac{\Delta V}{V_0}\right)^{t>t_x} = \beta_s \dot{f} t + \frac{2\pi r_{peak}^3 N_1}{3}\left[1 + \frac{\chi(t)}{\chi(t_{knee})}\right] + \left[\frac{3kT}{8\pi\gamma}\left(m_{obs} + \frac{\beta\dot{f}te^{\phi t}(1-\chi(t)/2)}{N_2}\right)\right]^{1/2}, \quad (52)$$

where β_s is the fractional swelling due to solid fission products per unit fission density.

3. Comparison with data

Fig. 4 shows the fission density at which the knee occurs obtained from a numerical solution of Eqs. (8)–(11) using Mathematica (http://www.wolfram.com) and the value of $R_{ds} = 0.42$ (derived in Section 2.3.2) as a function of fission rate compared with the experimentally estimated quantities [15]. The uncertainty in the experimental values is estimated to be ±20%. The results of Fig. 4 demonstrate that the theory is in agreement with the trends of the data. The fission density at which the knee occurs given by the analytical approximation of Eq. (21) is proportional to the square root of the fission rate. The analytical solution is also shown in Fig. 4. Eq. (21) is dependent on the validity of the approximate solution to Eq. (8) as given by Eq. (14). Fig. 5 shows a comparison between c_g calculated from a numerical solution to Eqs. (8)–(11) and c_g calculated with Eq. (14) as a function of irradiation time for three values of the fission rate. Also shown in Fig. 5 is the calculated position of the knee. It is clear from Fig. 5 that the approximate solution given by Eq. (14) approaches the numerical solution at irradiation times near the time required to achieve the knee. It is also interesting to note from Fig. 5 that the knee shifts to shorter times (and, as shown in Fig. 4, higher fission densities) as the fission rate is increased. Examination of the calculated quantities in Fig. 5 supports the validity of Eq. (14). Comparison of the calculated quantities and the data shown in Fig. 4 demonstrates that the theory follows the trend of the observation.

Fig. 6 shows the calculated fraction of generated gas in SEM-observable bubbles at the knee (i.e.,

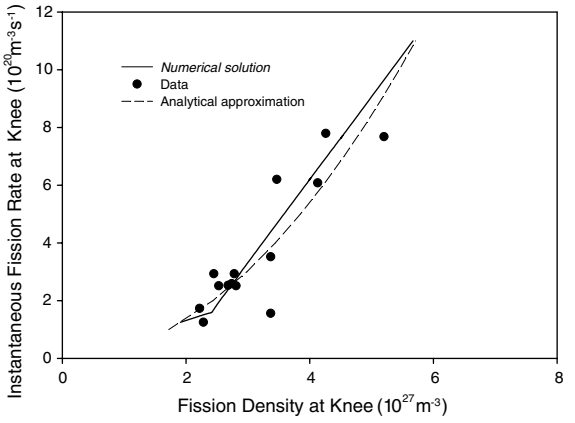

Fig. 4. Calculation of the fission density at which the knee occurs compared with data.

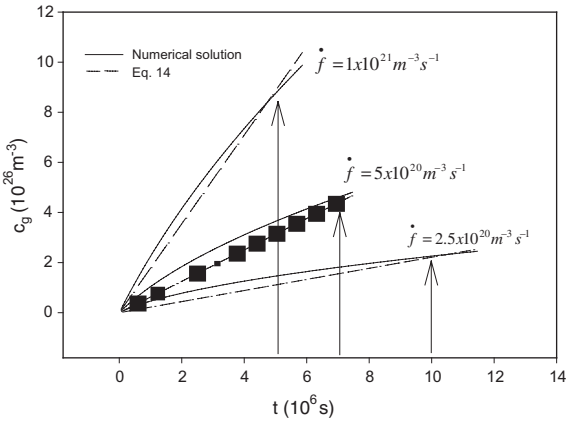

Fig. 5. Comparison between c_g calculated from a numerical solution to Eqs. (8)–(11) and c_g calculated with Eq. (14) as a function of irradiation time for three values of the fission rate. Also shown is the calculated position of the knee (arrows).

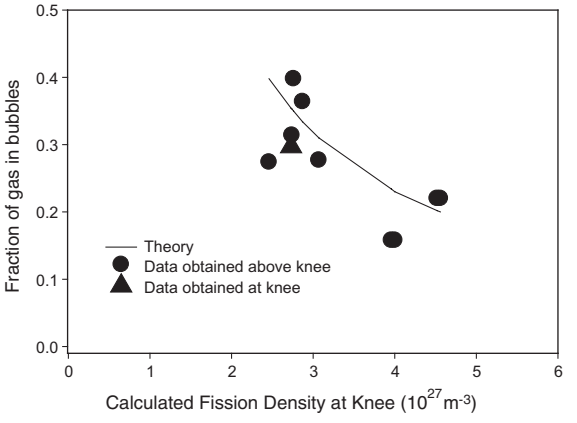

Fig. 6. Calculation of the fraction of generated gas in bubbles at the knee compared with data taken at various fission densities.

$m(\text{obs}) * N_2/\beta\dot{f}t$) made using Eqs. (22), (41), (43), (45) and (46) subsequent to the solution of Eqs. (8)–(11) compared with data taken at various fission densities [15]. The general agreement between the calculated and measured quantities supports the position that the gas in bubbles at times subsequent to the formation of the knee is relatively constant. This situation is possible due to the presence of the large bubble population formed at the knee which accumulates the generated gas concurrently with the evolution of the nanometer sized bubble population that inhabits the spaces in between the larger bubbles.

Table 2 shows the calculated average bubble diameter (Eqs. (11) and (46)) and density (Eq. (45)) at the knee compared with data for mini-plate A224 [15]. The calculated quantities are in agreement with the measured

Table 2
Calculated average bubble diameter and density compared with data for mini-plate A224 [15]

	Bubble diameter (μm)	Bubble density (10^{19} m^{-3})
Data	0.1	7.5
	0.15	0.85
Theory	0.116	7

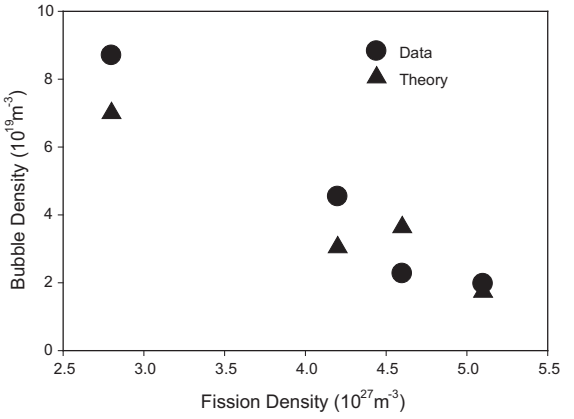

Fig. 7. Bubble density calculated using Eq. (50) compared with data.

values. Fig. 7 shows the calculated bubble density (Eq. (50)) as a function of fission density compared with data. The points at the lowest fission density are at the knee, whereas the other points are beyond the knee. It is important to note that aside from the time dependence inherent in Eq. (50), the density of bubbles at the knee N_2 is dependent on the fission rate (N_2 increases as the

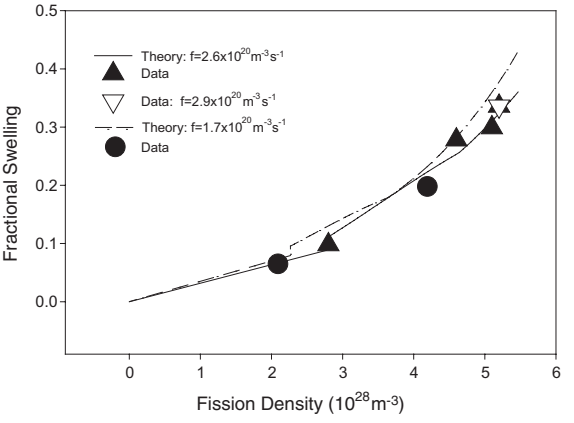

Fig. 8. Calculated fuel-particle swelling using Eqs. (49) and (52) for several values of the fission rate compared with data.

fission rate decreases, e.g. see Eq. (45)). The calculated results plotted in Fig. 7 show that in general, the bubble density decreases with continued irradiation (i.e., due to bubble coarsening by bubbles growing into each other) and follow the trend of the data.

Fig. 8 shows the calculated fuel particle swelling using Eqs. (49) and (52) for several values of the fission rate compared with data [15]. As is shown in Fig. 8, the knee in the swelling curve is defined by the increased slope due to the formation of the SEM-visible bubbles at the knee. The calculations shown in Fig. 8 indicate that higher fission rates result in decreased values of fuel swelling. The calculated swelling follows the trends of the data.

4. Discussion and conclusions

The fission rate dependence exemplified in Fig. 4 derives primarily from the gas bubble nucleation model wherein bubble nucleation occurs within shear bands initiated around free volume regions with small gas–atom clusters that form within these regions susceptible to dissolution due to viscous forces. The bubble coarsening process depends on the materials viscosity and on irradiation-induced gas–atom re-solution. For a material where bubble growth due to gas atom diffusion dominates that due to bubble motion and coalescence (e.g., as occurs in U_3Si, see Ref. [15]), the bubble distribution eventually reaches a point where larger bubbles from the tail of the evolving lognormal size distribution begin to contact the more numerous nanometer-sized bubbles from the peak region. This condition defines the knee in the swelling curve. Subsequent to the formation of the knee the above process repeats, but now the evolution of the nanometer size bubble distribution is overlaid on the pre-existing larger bubble population. Both bubble distributions coarsen due to the accumulation of fission gas as the irradiation proceeds. Eventually, a secondary knee point is achieved and a second population of bubbles in the tenths of a micron size range is generated. Thus, as the population of larger bubbles formed at the primary knee has coarsened, a bimodal population of bubbles is observed subsequent to the secondary knee point.

The validity of an evolving lognormal bubble-size distribution in an irradiated amorphous material that coarsens by bubbles growing into each other supported by the observation of nanometer sized helium bubbles that form, grow, and coalesce during low-temperature helium implantation in an amorphous alloy [12].

The spatial distribution of larger bubbles formed at the knee by coalescence of clusters of smaller bubbles growing into each other mirrors the spatial distribution of the bubble-size distribution prior to the knee, but on a larger length scale. Thus, as the irradiation proceeds, larger bubbles situated in relatively close proximity will grow into each other and coalesce. The rate of swelling increases at the knee due to the large bubble coarsening process. The swelling of high enriched U_3Si_2 intermetallic compounds to very high fission density is complicated by the changing chemistry of the material, specifically the decreasing uranium to silicon ratio. As the uranium is burned up and the U/Si ratio decreases, the gas–atom diffusivity of the material decreases (i.e., the viscosity increases) leading to a decrease in the swelling rate [15]. A quantitative description of this process is required in order to calculate the swelling of these materials to very high fission densities (e.g., fission densities $>6\times10^{27}$ m^{-3}).

The irradiation-induced swelling behavior of an amorphous material is primarily dependent on the materials viscosity. For values of the viscosity substantially smaller than that used in this work for the intermetallic compound U_3Si_2 (see Table 1), bubble diffusion will be fast enough such that bubble coarsening will occur due to bubble motion (i.e., the last terms on the right-hand-side of Eqs. (9) and (10) will dominate behavior) and will pre-empt the formation of a knee. An example of this type of material is irradiated U_3Si [16].

Acknowledgements

Work supported by US Department of Energy, Office of Arms Control and Nonproliferation, under Contract W-31-109-Eng-38.

References

[1] J. Rest, G.L. Hofman, J. Nucl. Mater. 210 (1994) 187.
[2] R.C. Birtcher, J.W. Richardson, M.H. Mueller, J. Nucl. Mater. 230 (1996) 158.
[3] R.C. Birtcher, J.W. Richardson, Private communication, Argonne National Laboratory, 1996.
[4] A. van den Beukel, Scr. Metall. 22 (1988) 877.
[5] A. Barbu, M. Bibole, R. Le Hazif, S. Bouffard, J.C. Ramillon, J. Nucl. Mater. 165 (1989) 217.
[6] S. Klaumunzer, C. Li, G. Schumacher, Appl. Phys. Lett. 51 (1987) 97.
[7] A.S. Argon, Acta metal. 27 (1979) 47.
[8] D.R. Olander, Fundamental aspects of nuclear reactor fuel elements TID-26711-PI-ERDA, 1976.
[9] A.H. Cottrell, The Mechanical Properties of Matter, John Wiley, New York, 1964.
[10] J. Rest, G.L. Hofman, J. Nucl. Mater. 277 (2000) 231.
[11] X. Chen, R. Birtcher, S.E. Donnelly, Mater. Res. Symp. Proc. 540 (1999) 331 (figure replicated with permission of the authors).
[12] H. Van Swygenhoven, L.M. Stals, G. Knuyt, J. Nucl. Mater. 118 (1983) 125.
[13] M.V. Speight, J. Nucl. Mater. 38 (1971) 236.
[14] Hj. Matzke, J. Nucl. Mater. 189 (1992) 141.

[15] M.R. Finlay, G.L. Hofman, J.L. Snelgrove, J. Nucl. Mater., in this issue.
[16] J. Rest, G.L. Hofman, R.C. Birtcher, in: N.H. Packen, R.E. Stoller, A.S. Kumar (Eds.), Proceedings on Effects of Radiation on Materials, 14th International Symposium, American Society of Testing and Materials STP, 1046, American Society of Testing and Materials, Philadelphia, 1990, p. 789.